

## NONLINEAR DYNAMIC BEHAVIOR OF PIPE-RESTRAINT SYSTEM

T. SHIMIZU, Y. SATO

*Hitachi Research Laboratory, Hitachi Ltd.,  
4026 Kuji-Machi, Hitachi-shi, Ibaraki-ken, 319-12, Japan*

T. YOSHINAGA

*Hitachi Works, Hitachi Ltd.,  
3-1-1 Saiwai-cho, Hitachi-shi, Ibaraki-ken, 317, Japan*

## SUMMARY

In this paper we mainly describe the results of an experimental study of pipe whip behavior under simulated BWR conditions. The experiments were aimed at determining whether the assumptions used in the design calculations of the pipe-restraint system were acceptable or not. In the experiments we used Type 304 stainless steel pipes (2-inch Sch 80) and U type rod restraints. Pipes and restraint strain were measured by strain gauges during blowdowns. Pipe whip behavior was recorded on a magnetic tape by a VTR instrument.

LOFT obtained experimentally a value of 30 degrees for the angle of spread of subcooled water steam jets. In the present experiments we also obtained a value of 30 degrees just after rupture, but this value decreased gradually to about 20 degrees 10 ~ 20 ms after rupture. The dynamic thrust forces resulting from steam jets were somewhere between  $1.62 Ap$  and  $1.26 Ap$ , where  $A$  denotes a cross sectional area of a pipe and  $p$  denotes static water pressure in a pipe. F. J. Moody (ASME-69-HT-31, August 1969) introduced the coefficient of  $Ap$  as 1.26 for real gas and 2.0 for cold water. According to our experimental results, the coefficient was much nearer to 1.62 than to 1.26. This means that restraints for piping should be designed to withstand a thrust force larger than  $1.62 Ap$ .

As far as pipe strains are concerned, the maximum strain occurred in the pipe regions supported by restraint rods. In other regions, between restraint locations and fixed edges, bending moment was almost uniform. There were two strain frequencies, 14 Hz and 100 Hz, one superposed on the other. The former frequency is apparently the second characteristic frequency of pipe bending and the latter is apparently the first characteristic frequency of longitudinal vibration of a rod. Almost all pipe strains were plastic ones. Some papers have assumed plastic hinges for a dynamic analysis of pipe whip behavior, but there were no plastic hinges in any part of the pipes used in our experiments. Thus, it appears that the dynamic analysis of pipe whip behavior in plastic regions will be complex.

The observation of pipe and restraint dynamic behavior with magnetic tape showed that the first restraint rod effectively absorbed pipe whip energy when a moment arm length was short, but that the second restraint rod did not work as well. Strain in the first rod was in the plastic region, but strain in the second rod was in the elastic region. On the other hand observation showed that the second restraint rod was very effective when the moment arm length was comparatively long. This was the case where the first restraint slipped along the pipe surface, because the rotation angle of a pipe tip was very large.

We also conducted experiments on the static deformation behavior of pipe-restraint system to obtain a constitutive equation for a pipe bending. Using this equation and curved beam theory, pipe whip dynamic behavior was analyzed.

## 1. Introduction

In the interest of public health and safety, nuclear power plant components are required to be protected adequately enough to ensure a safe reactor shutdown in the event of pipe breaks in the reactor pressure piping systems.

The reactor pressure piping systems of BWR's ( Boiling Water Reactor ) operate at 6.86 MPa ( 70 Kg/cm<sup>2</sup> ) and 288°C. If an instantaneous pipe failure was to occur in the piping systems, large thrust force would develop at the break area and result in unrestrained dynamic motion of the pipe. This uncontrolled pipe movement could result in severe damage to adjacent structure. Therefore a pipe restraint system has been developed and installed in the plants. In the event of a pipe break accident, the pipe restraint system interacts with the failed pipe and provides controlled movement of the pipe. Upon impact, the restraint stretches and the pipe bends about the restraint. Finally, a static equilibrium is achieved and the kinetic energy of the pipe is absorbed by the plastic deformation of the pipe and the restraint. This process, however, has not been observed and studied in experiments.

The purpose of our study is to understand the dynamic behavior of pipe restraint systems and to establish a design method for restraint hardware. Our programs are designed to demonstrate that a restraint is capable of limiting pipe movement under simulated BWR loading conditions and to evaluate the adequacy of analytical methods as design tools. In this report we describe the results of experiments and a theoretical analysis using ADINA.

## 2. Test Equipment

Figure 1 shows the arrangement of the pipe restraint system in the test facility. The pipes and restraints were fabricated from Type 304 stainless steel. They were scaled down to conform to the capabilities of test facility e.g., a 2-inch pipe was selected to represent an 8-inch water line. The function of a pipe restraint system is to capture a failed pipe and prevent damage caused by pipe whip. In Fig.2 a detailed drawing of a restraint is shown. A clevis is attached to each end of the restraint. A load bearing plate is fastened to the inner surface of the restraint to local buckling of the pipe wall. The whole assembly is connected to the lug by a pin. The test facility was constructed to meet thermodynamic requirements and to provide for the safety of operating personnel.

Figure 3 shows a general view of the test facility, which consists of the pressure vessel, fluid control system, the test stands in the exhaust tank and the pipe line with a rupture disk. The pressure gage located at the top of the pressure vessel measures water and steam pressure variation during blowdown events. There are some chromel-alumel thermocouples located inside the vessel to determine if the water temperature is uniform and at saturation temperature before blowdown. Figure 4 is a photograph of the

exhaust tank, showing the observation window and the silencers.

Figure 5 shows the pipe and restraint assembly on a test stand. The test stand consists of a concrete foundation to which a steel frame is fastened. The frame is subject to the reaction force of a jet thrust. There are 4 restraint rods in the test stand, as shown in the figure. Two of them are used in tests and two as back-up-restraints for safety.

### 3. Test Description

A VTR apparatus was used to observe the dynamic behavior of the pipe and restraints through the observation window. Six strain gages were installed on the restraint rods and the pipe was tested to measure dynamic strain during a blowdown as shown in Fig 6. A jet force was measured indirectly with gage No.3. The relation between the thrust force and the strain of gage No. 3 was obtained statically prior to blowdown. All strain gage outputs were recorded on light-beam type oscillographic recorders. The experimental parameters are summarized in Table 1.

Pipe restraint testing was divided into three categories

- (1) Investigation of the effects of clearance between the pipe and the restraints.
- (2) Investigation of the effects of the length of pipe overhang, from the restraint location to the free end.
- (3) Investigation of the effects of the rupture pressure of fluid.

For the first and second tests, vessel thermodynamic conditions were 4.41 MPa at 258°C. These were first category tests. For the third and fourth tests, the conditions were 6.86 MPa at 258°C. Dynamic strains were measured during testing and the final deformed shape of the pipe was investigated.

### 4. Test Results

Figure 7 shows the pressure variation of water in the pressure vessel for Tests 1,2 and 4. At the first stage of blowdown, vessel pressure increased slightly and, at the next stage, decreased about 10%. In Test 1 and 2 the vessel pressure decreased rapidly about 20 seconds after the jet started while in Test 4 the vessel pressure decreased gradually, earlier than in Tests 1 and 2. Figure 8 is a series of photographs of pipe motion during testing. These photographs were obtained from the screen of the VTR. The pipe began to deform almost immediately after the jet started.

The photographs indicate that the jet area expands to an angle of about 32° after 0.067 s. This value agrees closely with Loft's experimental results for subcooled water and stream blowdown. However, the angle reduces to about 20° after 0.2 s, which is the same as in Moody's assumption for saturated water and steam blowdown situations.

Figure 9 shows the variation of the thrust force for Test 4. This history was obtained from gage No. 3 using the calibration curve. Because of the coupled dynamic response of a load cell and piping, some errors might

be expected to occur in measurements. Therefore, gage was attached to the pipe, and no load cell was used. Thrust force is expressed by eq. (1)

$$T = K P_0 A_0 \quad (1)$$

where  $T$ : thrust force,  $P_0$ : initial pressure,  $A_0$ : pipe cross sectional area,  $K$ : non-dimensional thrust force.

In Test 4 the maximum thrust force which occurred at the instant when the pipe was captured by the restraint was 1.61 as shown in Fig. 9. This value is between those for solid water and ideal gas jets. The second thrust force peak appeared at a value 1.48 after 0.04 s. This is the time of the pipe impact on the second restraint.

Figure 10 shows the strain distributions along the pipe. The maximum plastic strain occurred at the point where the pipe was supported by the restraints (G.No. 4). The final deformation of pipes was measured after testing and is shown in Fig.11 for Tests 3 and 4. Displacement at the tip of the pipe is much larger for Test 3 than for Test 4. This is because the overhang length of the pipe for Test 3 is about 1.5 times that of the pipe for Test 4. This demonstrates that the overhang length affects pipe whip behavior very much. Plastic hinges did not occur at the pipe supported by the restraint in our experiments, we had to take this fact into consideration in establishing analytical models of the pipe-restraint system. Restraint strains are summarized in Table 2. We could not obtain detailed information about strain history because recorder trouble prevented us from obtaining strain values for Test 1. However no final extension of the restraint rods was found.

As shown in Table 2, the strains of restraint R1 which is located on the free-end side of the pipe are larger than those of restraint R2. This means that R1 is more effective than R2. The restraint rods were subjected to plastic strains caused by pipe whipping, but were strong enough to withstand them.

## 5. Theoretical Analysis

The finite element method was applied to analyze pipe whip behavior under experimental conditions. ADINA, which is a general purpose nonlinear static and dynamic finite element analysis program, was the computer program used. The pipe cantilever beam in Fig.12 was modeled as an assemblage of eleven 8-node isoparametric plane stress elements. In the numerical evaluation of the element matrices, 3-point Gaussian quadrature was used. The Wilson  $\theta$ -method, with equilibrium iterations in each time step, was used for direct time integration. The value  $5 \times 10^{-5}$  seconds was chosen as the time step increment. The mass of the pipe restraint system was lumped.

## 6. Solution Results

The following is an example of calculation results under experimental conditions for Test 4. A thrust force obtained by experiment was loaded

at the tip of the pipe model as a step function. Figure 13 shows pipe deformations at various time. Dynamic deformation of the pipe was not obtained in experiments, so we can not compare the calculation results with experimental results directly. But the calculated deformation seem to be large, comparing with the permanent deformation which was obtained by the experiment. The calculated deformation patterns agreed to the experimental result. As shown in Fig. 13, no local plastic hinge occurred. The pipe bent rather uniformly. Figure 14 shows the maximum stress distribution along the pipe. The calculated stress at the pipe portion supported by the restraint is about two times that of the experiment. The reasons of this difference between experimental and calculated results are supposed as the following. We used the infinitesimal deformation theory for the calculation, but the actual pipe deformation was pretty large. So stress and strain evaluation were poor. And we used the bi-linear stress-strain relation in such a way as calculated stresses would evaluate higher than real stresses. More significant reasons may be load condition and restraint model. The step load was used in the calculation which was the peak load in the experiment. Therefore the load for the calculation was probably overestimated. The experiments showed that the restraint located on the free-end side of the pipe was more effective as mentioned above, so only one restraint rod was modeled in the calculation. But the calculation result shows that the restraint should be modeled as two rods in the calculation which was done here.

## 7. Conclusions

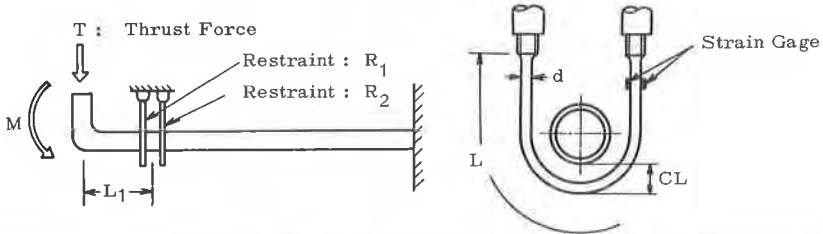
The following conclusions can be derived from calculations and the results of experiments.

- (1) The angle of jet area expansion is close to Moody's assumption for saturated water.
- (2) The influence of the clearance between the pipe and the restraint rod on pipe-restraint behavior was insignificant.
- (3) The overhang length of the pipe greatly affected pipe deformation. The longer the length of the overhang, the greater the deformation that occurred in the pipe. However strains in the restraint rods decreased with increasing overhang length.
- (4) The restraint nearest a pipe break works more effectively than the others at the instant of impact.
- (5) The design concept for the restraint rods which were used in the experiments is valid and sufficiently conservative for application to actual plant design.
- (6) Local plastic hinges did not occur in any portion of the pipes. Strain energy is distributed along the pipes. Pipe deformation patterns and strain distribution along the pipes agreed with the results of calculations.

References

- 1 Moody, F. J. "Prediction of Blowdown Thrust and Jet Forces" ASME paper 69-HT-31 ( Aug. 1969 )
- 2 Ma, S. M., Bathe, K. J., "On Finite Element Analysis of Pipe Whip Problems" Nuclear Engineering and Design, pp. 413-430 Vol.37 (1976)

Table I Experimental Parameters



T.P No.	Rupture Pressure Po MPa {kg/cm <sup>2</sup> }	Temperature (°C)	Clearance CL (mm)	Overhang Length L <sub>1</sub> (mm)	Restraint Rod Diameter d (mm)	Restraint Length B (mm)	Number of Restraints
Test 1	4.41 { 45 }	257.6	0	367	6	45	2
Test 2	" { " }	"	20	361	"	"	"
Test 3	6.86 { 70 }	284.5	"	365	8	55	"
Test 4	" { " }	"	"	211	"	"	"

Table 2 Test Results

Test	Max. Thrust Force T <sub>max</sub> KN {kg}	Max. Bending Moment M <sub>max</sub> KN·m {kg·m}	Re-straint	Peak Strain ( 10 <sup>-6</sup> )	Plastic Strain ( 10 <sup>-6</sup> )	Restraint Length before Test L <sub>s</sub> (mm)	Restraint Length after Test L <sub>e</sub> (mm)
1	—	—	R <sub>1</sub>	—	—	235.0	235.0
			R <sub>2</sub>	—	—	233.0	233.0
2	13.17 {1400}	4.95 {505}	R <sub>1</sub>	950	550	234.0	235.6
			R <sub>2</sub>	330	0	235.0	235.0
3	16.82 {1716}	6.10 {512}	R <sub>1</sub>	1150	800	272.3	274.0
			R <sub>2</sub>	250	0	272.0	272.0
4	21.21 {2175}	4.50 {375}	R <sub>1</sub>	2310	1700	263.2	264.5
			R <sub>2</sub>	120	0	264.0	264.0

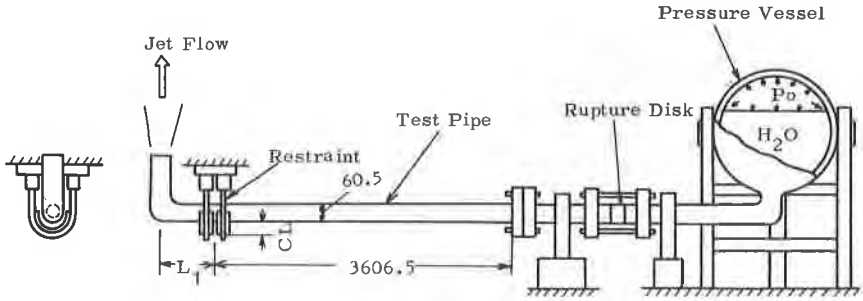


Fig. 1 Arrangement of Pipe and Restraint

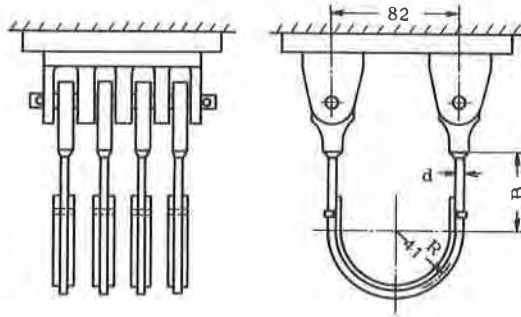


Fig. 2 Arrangement of Restraint

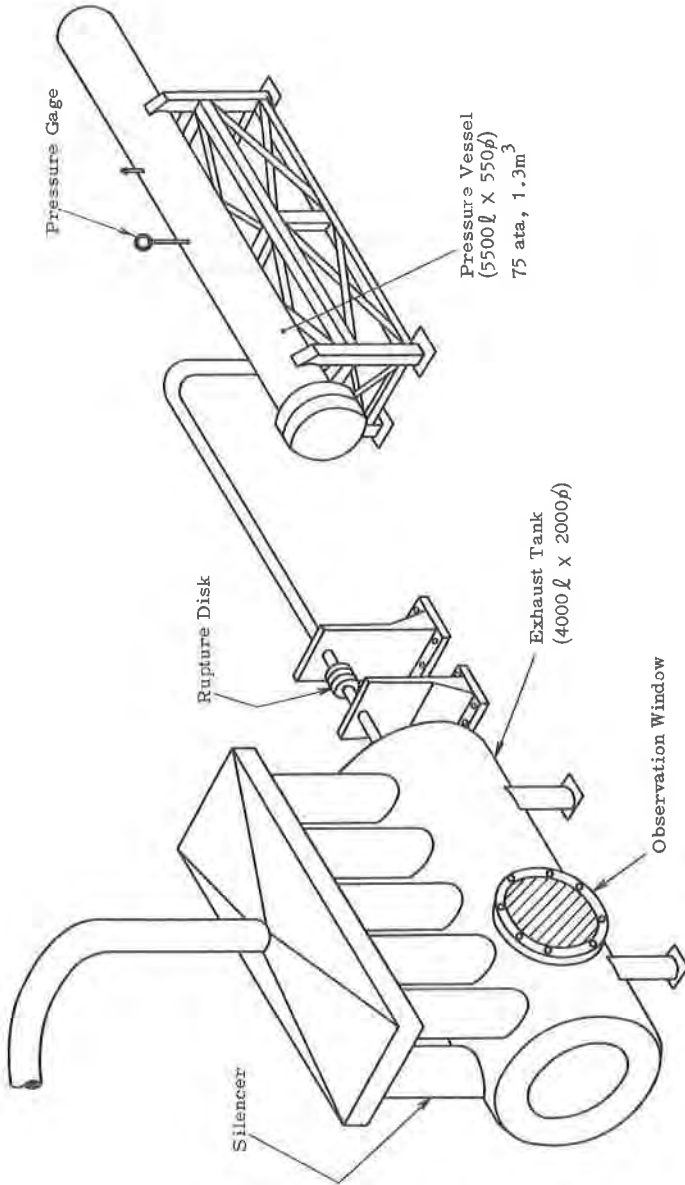


Fig. 3 General View of Test Facility



Fig. 4 Exhaust Tank

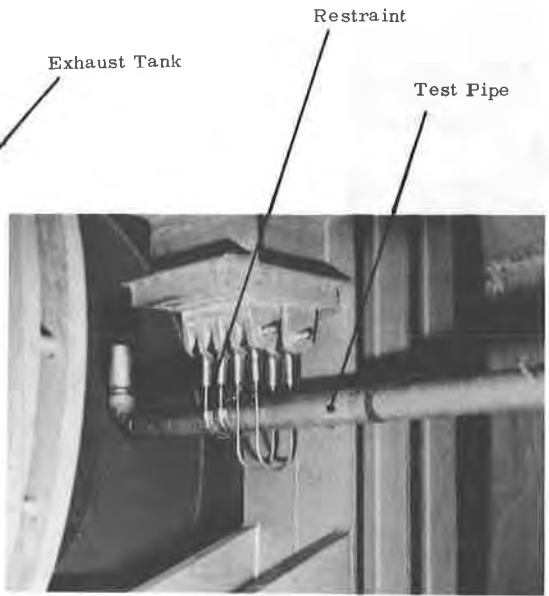


Fig. 5 Assembly of Pipe and Restraint

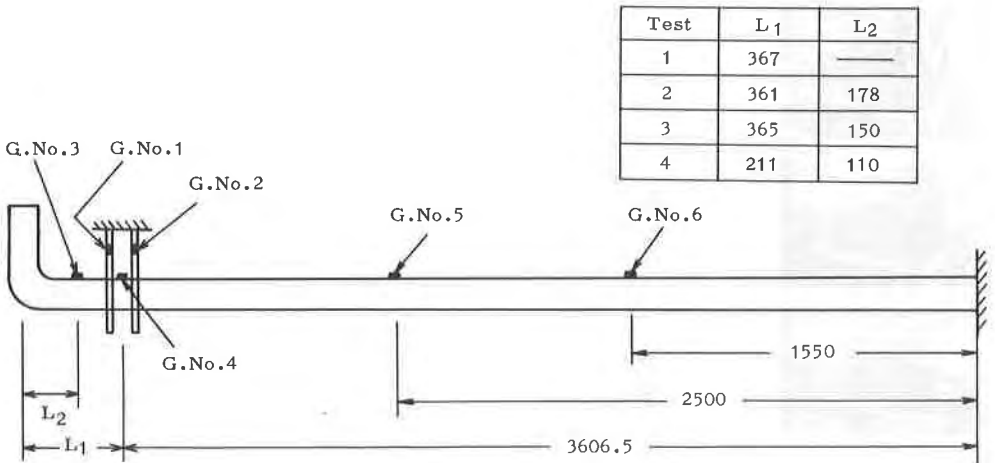


Fig. 6 Locations of Strain Gages

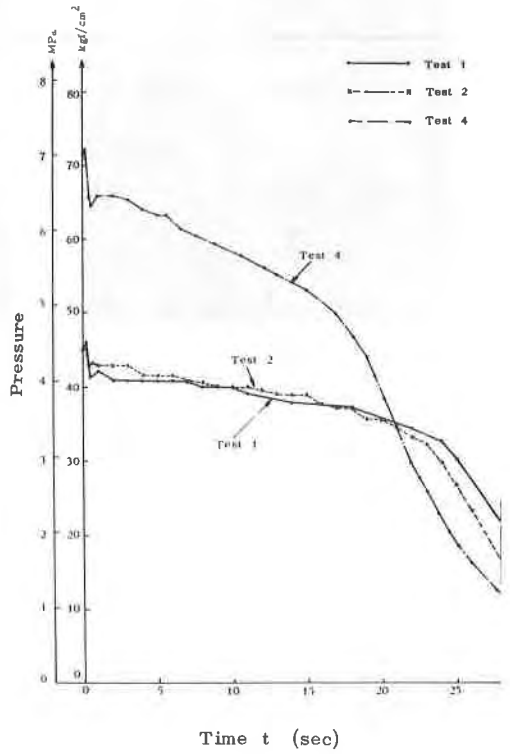
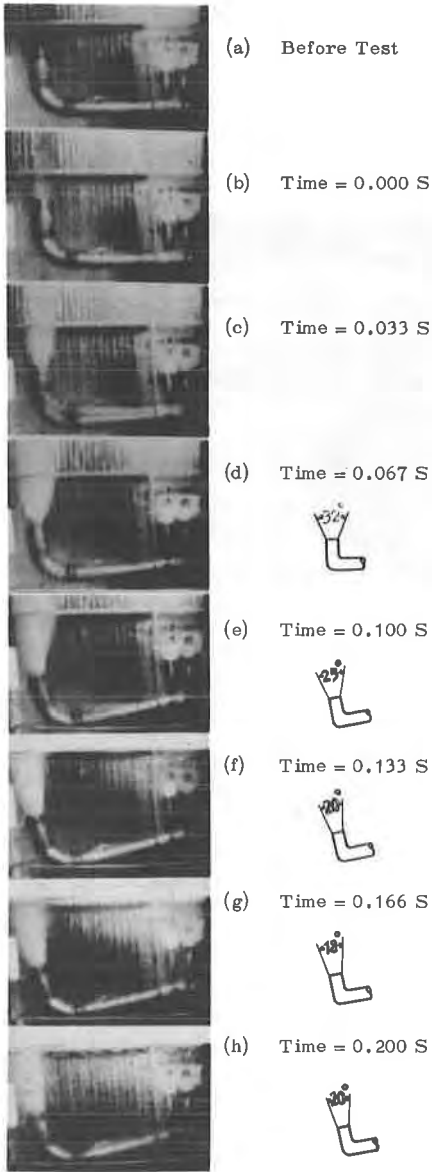


Fig. 7 Pressure Variation of Water in the Pressure Vessel

Fig. 8 Jet Flow and Pipe Motion (Test 3)

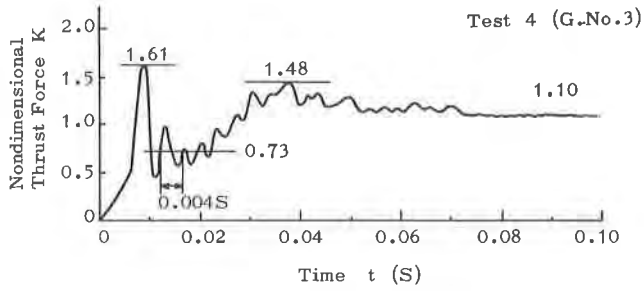


Fig. 9 Variation of Thrust Force with Time

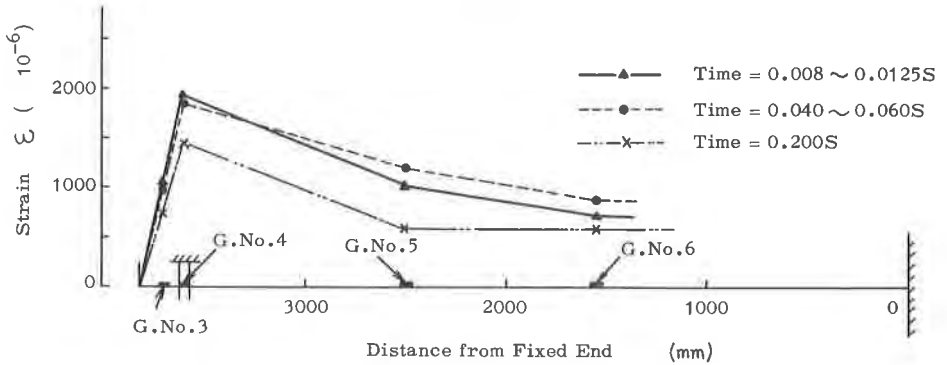


Fig. 10 Dynamic Strain Distribution along Pipe (Test 4)

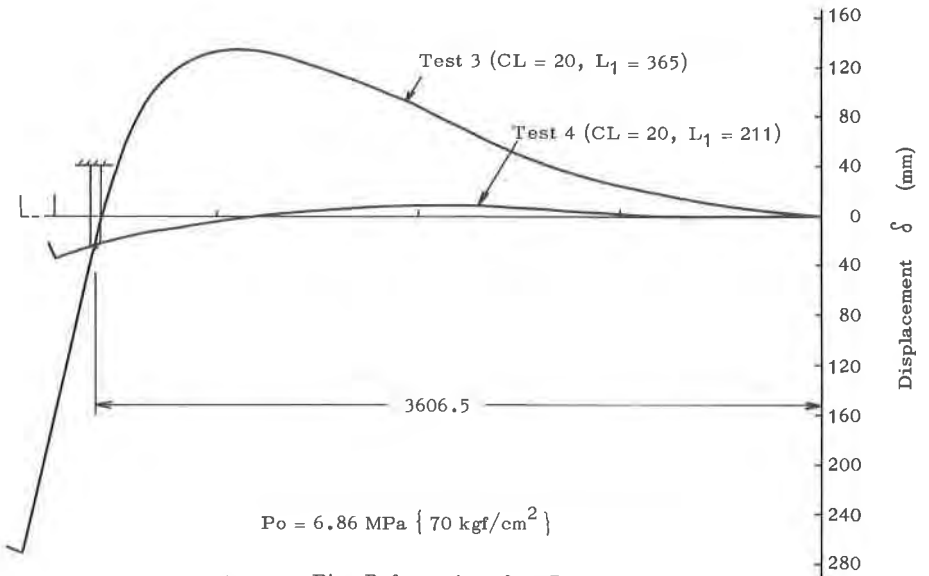


Fig. 11 Pipe Deformation after Test

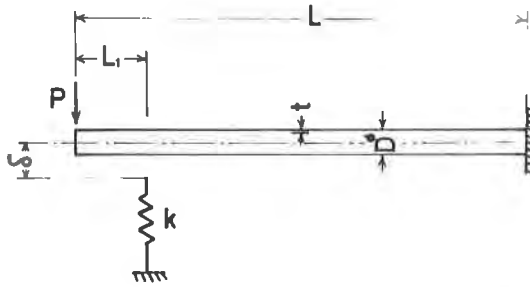


Fig.12 Analysis Model

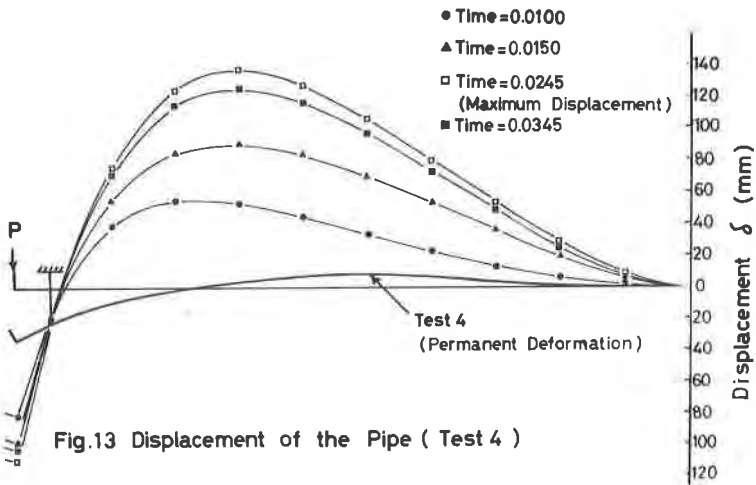


Fig.13 Displacement of the Pipe ( Test 4 )

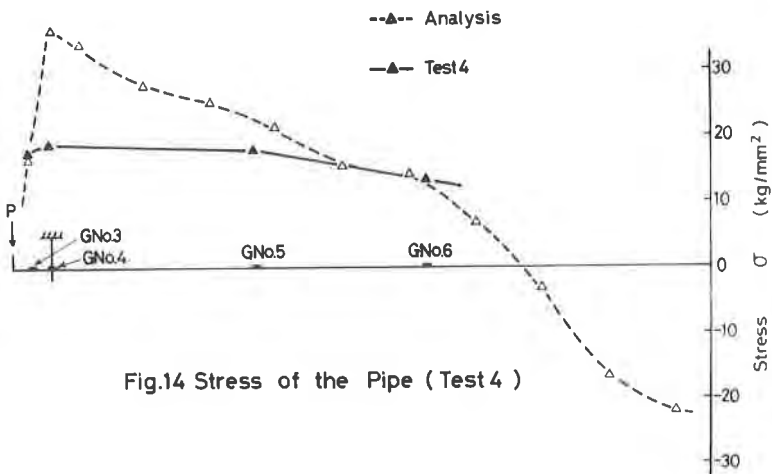


Fig.14 Stress of the Pipe ( Test 4 )